Solar Energy 297 (2025) 113612

Contents lists available at ScienceDirect

Solar Energy

journal homepage: www.elsevier.com/locate/solener

Smart design of hybrid solar-gas turbine plants for decarbonization: A multi-criteria optimization case study in the MENA region

Samir Hassani [a,*], Toufik Arrif [a], Mawloud Guermoui [a], Noureddine Yassaa [b,c], Abdelfetah Belaid [a], Rosa P. Merchán [d], Badraddine Bezza [a], Robert A.Taylor [e], Saad Mekhilef [f]

[a] *Unité de Recherche Appliquée en Energies Renouvelables, URAER, Centre de Développement des Energies Renouvelables, CDER, Ghardaïa, Algeria*
[b] *Commissariat aux énergies renouvelables et à l'efficacité énergétique (CEREFE) 23, Rue Dr Asslah Slimane, Telemly, Algiers, Algeria*
[c] *Faculty of Chemistry, University of Sciences and Technology Houari Boumediene, BP 32 El-Alia Bab-Ezzouar, Algiers, Algeria*
[d] *Department of Applied Physics and IUFFYM, Universidad de Salamanca, Salamanca, Spain*
[e] *School of Mechanical and Manufacturing Engineering, University of New South Wales, Sydney, NSW 2052, Australia*
[f] *School of Science, Computing and Engineering Technologies, Swinburne University of Technology, Hawthorn, VIC 3122, Australia*

A R T I C L E I N F O

Keywords:
Solar Tower
Gas Power Plant
Hybridization
Decision-Making Method
Low-carbon technologies
Energy Transition

A B S T R A C T

The integration of solar and gas turbine technologies through hybridization emerges as a promising approach to enhance the sustainability of power generation systems. However, the design process for such hybrid systems is challenging, particularly in terms of optimization and decision-making strategies. In this research, a case study of redesigning of an existing $7.2MW_e$ gas power plant by integrating a heliostat field and a central air receiver for preheating purposes has been presented. To accurately adjust the critical parameters of the hybrid solar gas power plant, a tri-objectives optimization approach was employed using two advanced optimization methods: Non-dominated Sorting Genetic Algorithm III and Multi-Objective Grasshopper Optimization Algorithm. Furthermore, the hybrid Fuzzy Analytic Hierarchy Process and The Technique for Order of Preference by Similarity to Ideal Solution decision-making method has been employed to help select the optimal design points from various scenarios and priorities. The chosen design for the hybrid solar-gas power plant showcases an efficient heliostat field footprint, a competitive LCOE of $78USD/MWh$, achieves an annual reduction in natural gas consumption by 13.8%, and mitigates CO_2 emissions by $81.6gCO_2/kWh$ ($\approx 715tCO_2/MW_e$,).Thus, this study presents a persuasive example of a low-carbon technological solution, offering a promising strategy for the ongoing energy transition in the Middle East and North Africa (MENA) region.

1. Introduction

Today's world confronts a pressing challenge regarding energy demand and supply. According to the World Resources Institute, WRI 2021 annual report [1], energy ranks among the top seven global challenges requiring urgent attention. Currently, fossil fuels, including oil, gas and coal, represent more than 80 % share of total energy consumption [2], where 61 % of electricity still comes from fossil fuels [3]. However, the combustion of fossil fuels produces a large carbon footprint, and it accounted for over 90 % of global CO_2 emissions in 2021 [4]. The largest rise in CO_2 emissions occurred in electricity and heat production, accounting for 46 % of the total growth in emissions [4]. Obviously, more efforts are still indispensable to promote the energy transition, decarbonization, and meet the Paris climate goals [5] and achieve 1.5 °C target [6].

The electricity generation using natural gas is a less polluting energy source than coal and oil. Therefore, several nations are either using or planning to utilize natural gas as a bridging/ transition fuel before net zero by around 2050. However, the pace of gas consumption nowadays may exhaust several natural gas fields before 2050. Therefore, hybridizing gas-fired power plants with renewable energy-based technologies is a highly recommended solution.

Comprehensive review papers on this topic have been authored by B. A. A. Yousef et al. [7], O. Achkari and A. El Fadar [8], Cardemil et al. [9], and M. Chitakure [10]. Typically, conventional power plants use fossil fuels as their primary heat source. When hybridized with zero or low carbon emission supplementary heat sources, these plants might experience a decrease in energy efficiency. However, this reduction in efficiency is offset by the advantages of decreased emissions and fuel

* Corresponding author.
E-mail address: s.hassani@cder.dz (S. Hassani).

https://doi.org/10.1016/j.solener.2025.113612
Received 6 February 2025; Received in revised form 6 May 2025; Accepted 17 May 2025
Available online 23 May 2025
0038-092X/

Nomenclature

Latin letters

A_{abs}	Absorber area [m^2]
A_{hf}	Heliostat land area [m^2]
A_{ref_field}	Heliostats field total reflective area [m^2]
A_{pp}	Original gas power plant area [m^2]
A_{sing}	Area of a single heliostat [m^2]
A_{tot}	Total land area owned by the company [m^2]
AF	Air-fuel ratio [-]
cf	A flow rate conversion factor [m^3/kg]
$c_{p,air}$	Air specific heat at constant pressure [-]
CRF	Capital Recovery Factor [-]
DNI	Direct Normal Irradiance [W/m^2]
d_{in}	Internal diameter of the receiver's tubes [m]
E_{ele}	Annual electrical energy [MWe]
f_s	Solar share factor [-]
H_{c_in}	Enthalpy of the air at the compressor entrance [kJ/kg. K]
H_{c_out}	Air enthalpy at the outlet of the compressor [kJ/kg. K]
H_{cc_out}	Outlet enthalpy of the combustion product mixture [kJ/kg. K]
h_{int_fc}	Heat transfer coefficient for internal flow forced convection [-]
H_{rec_out}	Enthalpy of the preheated air at the outlet of the receiver [kJ/kg. K]
H_{t_in}	Enthalpy of gas mixture at the turbine entrance [kJ/kg. K]
k_{air}	Thermal conductivity of air [-]
$LCOE$	Levelized cost of energy [USD/MW]
LHV	Lower Heating Value of natural gas [MJ/kg]
LUF	Land use factor [%]
$\dot{m}_{air}$	Air mass flow rate [kg/s]
$\dot{m}_{CH4}$	Natural gas mass flow rate [kg/s]
n_c	Compressor design speed [rpm]
N_{hel}	Number of heliostats [-]
Nu_D	Nusselt number [-]
n_t	Turbine design speed [rpm]
P_{inc}	Incident solar radiation on the receiver [kw]
P_{s_field}	Total solar radiation incident on heliostat field [W/m^2]
$\dot{Q}_{abs}$	Net solar power absorbed by the receiver [kJ]
$\dot{Q}_{loss}$	Combined losses of conduction, convection, and thermal radiation [kw]
r_p	Pressure ratio [-]
T_{air_avg}	Average temperature of the air in the receiver [$^\circ C$]
T_{amb}	Ambient temperature [K]
T_{c_out}	Temperature at the outlet of the compressor [K]
T_{int_cav}	Temperature at the internal cavity receiver [K]
T_{rec_out}	Temperature at the outlet of the receiver [K]
T_{t_in}	Turbine inlet temperature [$^\circ C$]
T_{t_out}	Turbine outlet temperature [$^\circ C$]
TH	Solar tower height [m]
U_L	Overall convective and conductive heat transfer coefficient [-]
V_{CH4_con}	Annual natural gas consumed by the original gas power plant [m^3]
V_{s_CH4}	Annual volume of natural gas saved [m^3]
$\dot{W}_e$	Net electrical power produced [MW]
$\dot{W}_t$	Turbine power [MW]
Z_{inv}	Total investment costs [USD]
$Z_{O\&M}$	Annual operations and maintenance costs [USD]

Greek Letters

α_{eff}	Effective emissivity of the internal cavity receiver [-]
α_{rec}	Absorption efficiency of the absorber material [-]
γ_{air}	Specific heat ratio of air [-]
γ_{gas}	Specific heat ratio of gas [-]
η_{att}	Atmospheric attenuation efficiency [-]
η_c	Receiver Isentropic efficiency (thermal efficiency) [-]
η_{cc}	Combustion efficiency [-]
η_{cos}	Cosine efficiency [-]
η_{field}	Heliostat field instantaneous optical efficiency [-]
η_{hel}	Instantaneous optical efficiency of a heliostat [-]
η_{int}	Interception efficiency [-]
η_{ref}	Mirror reflectivity efficiency [-]
η_{sb}	Shadowing and blocking efficiency [-]
η_t	Turbine Isentropic efficiency [-]
$\eta_{yearly,I}$	Heliostat field yearly weighted optical efficiency [-]
σ	Stefan-Boltzmann constant (5.670374419 × 10^{-8}) [W / (m^2 x K^4)]
ΔR_i	Radial distance between heliostats rings [m]
Δaz_i	Azimuth angular spacing between adjacent heliostats [$^\circ$]

Acronyms

AHP	Analytic Hierarchy Process
CSP	Concentrated Solar Power
GA	Genetic Algorithm
HFLCAL	Heliostat Field Layout Calculation
MOPSO	Multi-Objectives Particle Swarm Optimization
MOGOA	Multi-Objectives Grasshopper Optimization Algorithm
NSGA-III	Non-Sorted Genetic Algorithm
PESA-II	Pareto Envelope-Based Selection Algorithm
SPEA2	Improving the "Strength Pareto Evolutionary Algorithm".
STEC	Solar Thermal Electric Components
TOPSIS	Technique of Order Preference Similarity to the Ideal Solution
TRNSYS	Transient Systems Simulation Program
REFPROP	REFerence fluid PROPerties
WRI	World Resources Institute

savings, as demonstrated by T. Yue, N. Lior [11]. Furthermore, adding the thermal output from concentrated solar power (CSP) plant's solar field to an existing conventional power plant is one of the main conceivable cost-effective method for hybridizing CSP-fossil fuel power plants [12].

Buck et al. [13] proposed a pressurized volumetric air receiver for hybrid solar tower and gas turbine application. The results showed that the air receiver exit temperature reached 815 °C with an efficiency of up to 70 %. The study recommended that such hybrid technology could be competitive with conventional plants.

The solar-powered gas turbine hybrid system concept has been experimented for the first time under the SOLGATE project in Spain [14–16]. The main project's objective was to design a pressurized air receiver that could provide heated air up to 1000 °C for direct use in a gas turbine [17].

P. Schwarzbozl et al. [18] conducted a study on the cost-efficient design of solar-hybrid gas turbine plants with varying power outputs, and locations. Using the HFLCAL code for heliostat field design and TRNSYS with STEC for performance simulation, they found annual efficiencies ranging from 35.9 % to 40.4 %, with a solar share of 38 % to 75 %. The study indicates that smaller plants (≤16 MWe) with remote operation can achieve solar electricity costs below 10 €cent/kWh.

R. Buck, et S. Friedmann [19] have presented a thermal and economic study of a solarized 100kWe microturbine. The electric efficiency of the hybrid system has been found lower by 2 % compared to the original microturbine without solar hybridization. However, the solar share made a significant contribution to fuel savings. In addition, it has been found that such hybrid technology can produce electricity at 92 €/MWh.

P. Heller et al. [14] have tested the first prototype of solar powered gas turbine system at CESA-1 tower facility in Spain. The test results showed that the pressurized air temperature at the combustor air inlet provided by the air receiver reached 960 °C. The amount of produced electrical power was 165kWe with 70 % solar contribution.

In a similar project namely PEGASE, where a theoretical hybrid solar gas turbine system was simulated by P. Garcia [20]. A centrale air receiver was used to heat up pressurized air at 850 °C, then a combustion chamber has been employed to burn the mixture air–fuel producing gas at 1000 °C. According to the study's outcome, the collected solar energy at the central receiver system could provide 62 % of the required thermal power to the gas turbine.

SOLUGAS project, implemented in Spain, and presented by R. Korzynietz et al., [21] has been proposed to demonstrate the feasibility of the first megawatt scale hybrid solarized gas turbine power plant. This project has applied a tubular air receiver proposed earlier by the same author [22]. The hybrid plant has undergone more than 1000 operation hours, and the receiver outlet temperature reached 800 °C. Under ISO conditions, the anticipated open cycle efficiency has been found to be 27 %. To increase the hybrid plant efficiency, it has been recommended to add a bottoming cycle to recover the waste heat from exhaust gas turbine.

Hischier et al. [23] have analyzed and compared the thermal performance of three thermodynamic cycles namely, Brayton, recuperated Brayton, and combined Brayton-Rankine cycles. A 50 MW solar power tower was used as the main source of energy, where a cluster of solar receiver modules has been used. The numerical results demonstrate that a 37 % of solar-to-electricity efficiency is achievable. However, the shading/blocking efficiency has not been considered in their analysis.

M.J. Santos et al. [24] have proposed a single step recuperative closed Brayton cycle hybridized with a solar tower. The thermodynamic model has been validated against data from SOLUGAS project [25]. The authors claimed that a hybrid gas central solar tower plant with recuperative system could save 11.7 % of fuel during summer season against 8.7 % without recuperative mode. An improved version of the thermodynamic model has been proposed by R.P. Merchán et al. [26] to evaluate a hybrid thermosolar central tower Brayton plant in terms of annual performance and emissions. The authors concluded that in the case of real operating conditions with recuperation the solar share has been found to be 0.164. However, yearly fuel consumption and emissions have been lessened by 8.313 %. In a recent work done by the same authors [27], a thermo-economic and sensitivity analysis of a solar tower hybrid Brayton cycle power plant has been presented. The authors concluded that turbine inlet temperature, and solar receiver aperture size are the most affecting parameters on levelized cost of energy (LCOE) output values.

J. Yang, G. Xiao, M. Ghavami et al. [28] have developed a mathematical model along with a control strategy to assess the thermodynamic performance of a solar micro gas turbine with thermochemical energy storage. The results show that, this control strategy guaranteed a stable power production of 12.6 $kW_e \pm 5$ % under 750–820 W/m^2. The co-authors G. Xiao et al. [29] in another study have combined a micro solar gas turbine with steam injection and organic Rankine cycle. Four typical days of the year have been considered to evaluate the system. The simulation results showed that a maximum fuel consumption reduction of 24.6 % can be achieved during summer solstice.

Amani & Ghenaiet [30] have carried out a multi-objective optimization population-based GA of a hybridized combined Brayton-Rankine cycle power plant with a solar tower plant. The results showed that the net solar energy ratio may reach up to 23.5 %, and the levelized cost of energy could be reduced by 16 %. In addition, over 30 years of operating service the hybrid plant may reduce emissions by 0.33 million tonnes.

A. Ahmadi, M.A. Ehyaei, D.H. Jamali et al. [31] investigated the energy, exergy, and economic performance of a hybrid thermodynamic power plant under two configurations with (referred as System 1) and without (referred as System 2) integration of solar heliostat receiver. Authors reported that in terms of economical point of view system 2 has been found less profitable by 21 % against system 1. The main reason behind this low economic performance of the system 2 could be attributed to the weak optimization of the heliostat field and air-receiver parameters.

S.M. Alirahmi et al. [32] proposed a hybrid cogeneration plant for electricity, freshwater and hydrogen production. The exhaust gas exiting high pressure turbine is reheated using a solar tower before entering a low-pressure turbine. A multi-objective optimization has been made using NSGA-II, MOPSO, SPEA2, and PESA-II. By using TOPSIS technique for best trad-off solution, the optimization output provided an optimum for the total cost rate and exergy efficiency of 224.1 $/h and 26.7 %, respectively.

J. García-Ferrero et al. [33] conducted a study on the incorporation of Brayton technology in both central tower plants and parabolic dish farms across three different global locations. Although the technical outcomes appeared highly promising, the financial analysis showed that central tower plants demand more significant investments than parabolic dish farms. R Ghasemiasl et al. [34] explored a solar-hybrid cogeneration cycle that combines a heliostat-based solar system with a 25-MW gas turbine, aiming to produce both electricity and freshwater across various locations. The innovative system has the potential for an annual fuel saving of approximately USD 2.4 million, and electricity generation rate at 86.9 USD/MWh. F. Rovense et al. [35] analyzed the off-design performance maps of a micro gas turbine when integrated into a Concentrating Solar Power. The findings revealed that increasing the turbine inlet pressure, coupled with increased solarization that raises the turbine inlet temperature to 850 °C, can yield a net power output of up to 570 kWe and achieve an efficiency of 34 %. Recent literature has offered interesting insights into the application of microturbines in concentrated solar power. To advance sustainable energy systems through solar integration, Hemmatpour et al. [36] optimize a gas-solar cogeneration cycle that produces electricity and fresh water. Using PSO optimization method, they achieve a 0.5 % increase in energy efficiency, and a 1 % reduction in exergy destruction. Similarly, Ghasemiasl et al. [37] expand the scope to a multigeneration system, integrating solar power with combined cycle power plants to produce electricity, water, and hydrogen. Their approach reduces emissions by 9.8 % and yields annual fuel savings of $8.7 million.

Noteworthy studies on this subject have been reported by R De Robbio [38] and Jingqi Li et al. [39].

1.1. Main scope and Contributions of this study

Based on our literature survey, there are limited real-case studies on hybrid solar tower gas power plants that focus on multi-objective optimization and the application of multi-criteria decision-making methods for optimal design. Therefore, in this study, an existing gas-fired power plant has been redesigned through the integration of heliostat field and central air receiver for preheating propose. In addition, this study pioneers the application of the NSGA III and the MOGA for multi-objective optimization in the context of solarized gas power plants design. Moreover, to effectively identify the optimal trade-off design option among various scenarios and priorities, this study, to the best of the authors' knowledge, represents the first utilization of a hybrid multi-criteria decision-making approach within the context of solarized gas power plant design. This novel approach, developed in this study, simultaneously combines the Fuzzy Analytic Hierarchy Process with the Technique for Order of Preference by Similarity to Ideal Solution

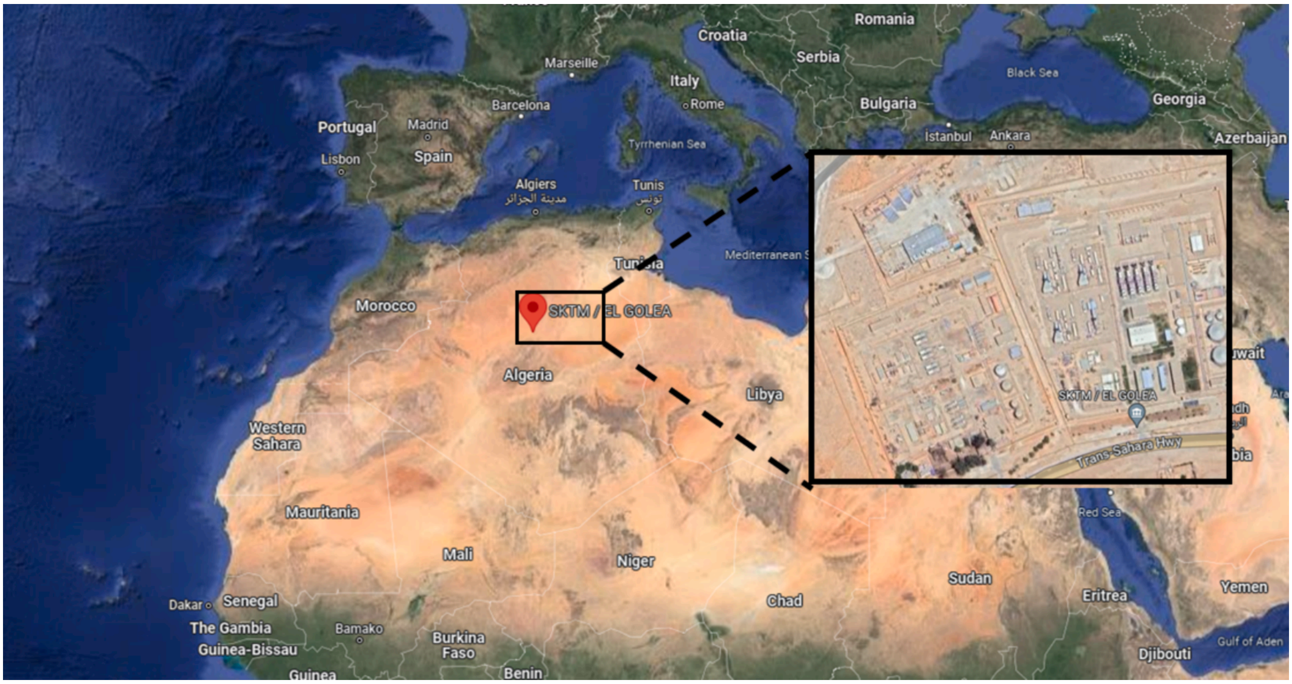

Fig. 1. Location Map of the Project Site.

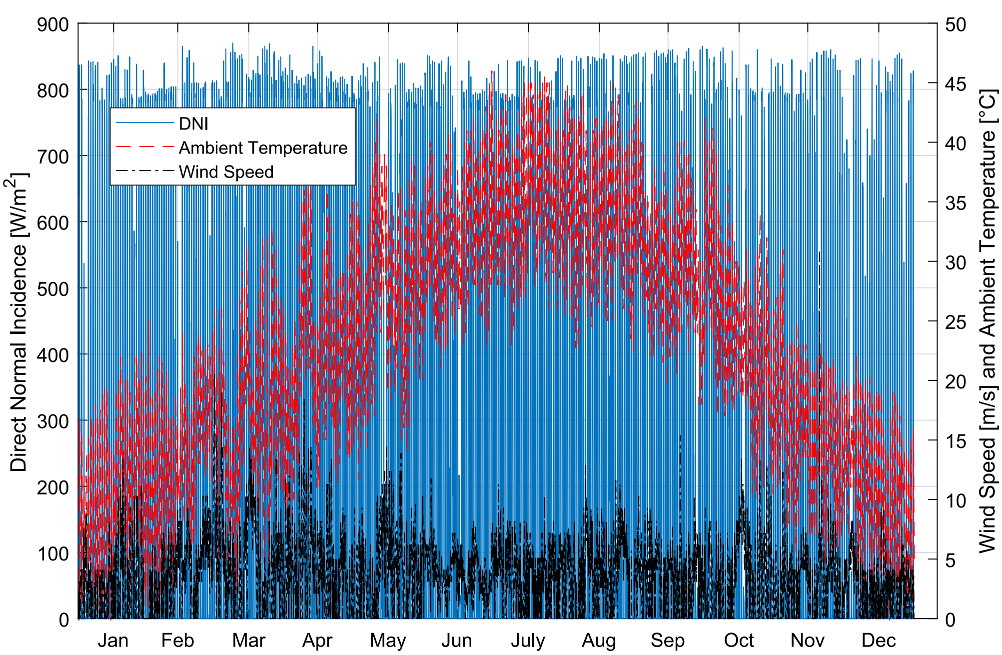

Fig. 2. Actual hourly weather characteristics of the selected location based on typical meteorological years from 2004 to 2018.

methods. Furthermore, the ingenious design strategy that integrates these two advanced methods – multi-objective optimization and multi-criteria decision-making – constitutes a significant innovation in the field. It enables the design of an optimal solar gas power plant characterized by low carbon emissions, competitive LCOE, minimal land footprint, and reduced natural gas consumption. This contribution not only advances the field but also addresses a critical gap in existing literature on solarized gas power plants.

2. Concept implementation and location selection

The selection of the gas power plant location was based on specific criteria, including favorable weather conditions for CSP technology and proximity to open areas suitable for installing a heliostat field. It was essential to avoid residential areas and arable land. Therefore, a 7.2 MWe gas power plant located in El Menia province in the south of Algeria was chosen for this study. The GPS coordinates of the power plant are 30°36′27.4″N 2°54′07.4″E, as shown in Fig. 1.

The chosen location exhibits a high annual Direct Normal Irradiance (DNI) of 2205.4 kWh/m^2 , making it highly favorable for the deployment of on-grid CSP [40]. The weather conditions used in various calculations for this study are depicted in Fig. 2 and are based on Typical Meteorological Years from 2004 to 2018, sourced from the local meteorological station and available online at Climate.OneBuilding.Org [41].

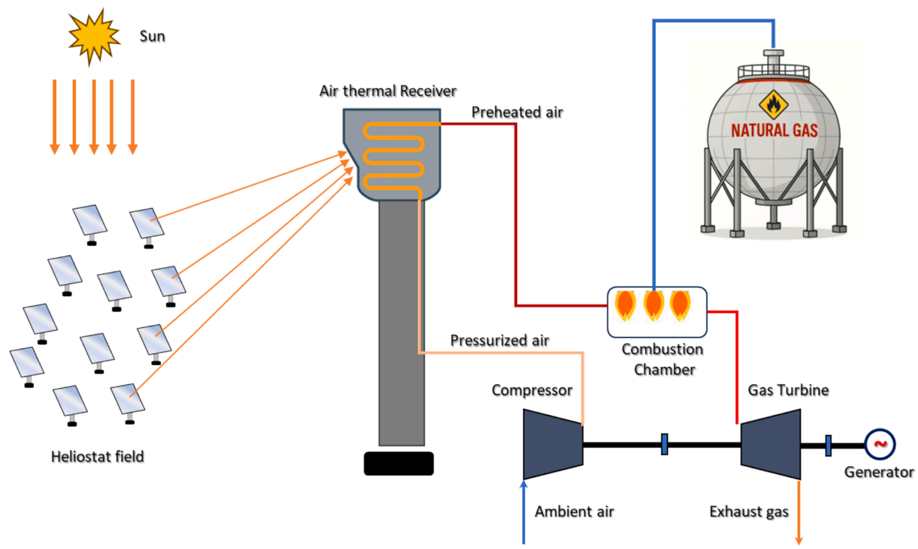

Fig. 3. Layout of the integrated solar tower in a gas power plant. The system consists of a heliostat field and a pressurized air receiver, a combustion chamber, and a gas turbine.

3. Methods

This study developed a comprehensive numerical model to design and assess the proposed hybrid solarized gas power plant. The model includes the heliostat field, thermal receiver design, turbine performance, and economic analysis for calculating energy cost.

3.1. Working principle of the proposed hybrid system

The hybrid solar gas power plant operates by using a solar tower, heliostat field, and central receiver to partially supply the thermal power needed to heat the working fluid at the turbine inlet. This method decreases natural gas usage in the combustion chamber, thereby reducing emissions. The hybrid system's detailed layout is shown in Fig. 3.

When solar radiation is insufficient (e.g., at night or during cloudy periods), the hybrid system operates in conventional gas turbine mode, relying solely on natural gas combustion to heat the air to the required turbine inlet temperature.

3.2. Receiver thermal model

The central receiver considered in this study is a pressurized cavity tubular air receiver, similar to the one used in the SOLUGAS project [21]. To evaluate its thermal performance, particularly the enthalpy of the preheated air at the outlet of the receiver H_{rec_out}, a thermal model was developed based on the first law of thermodynamics i.e., the energy balance equation. The determination of H_{rec_out} is done using equation (1).

$$H_{rec\_out} = H_{c\_out} + \frac{\dot{Q}_{abs}}{\dot{m}_{air}} \tag{1}$$

$\dot{m}_{air}$ is the air mass flow rate, and H_{c_out} is the air enthalpy at the outlet of the compressor evaluated based on the outlet temperature T_{c_out} determined using equation (2):

$$T_{c\_out} = T_{amb} \times \left(1 + \left(\frac{1}{\eta_c}\right) \times \left(r_p^{\left(\frac{\gamma_{air}-1}{\gamma_{air}}\right)} - 1\right)\right) \tag{2}$$

$\dot{Q}_{abs}$ is the net solar power absorbed by the receiver, representing the useful thermal power added to the air for preheating before entering the combustion chamber. The $\dot{Q}_{abs}$ is highly dependent on the quality of insulation and the optimal geometry design of the cavity receiver.

$$\dot{Q}_{abs} = \alpha_{rec}.P_{inc} - \dot{Q}_{loss} \tag{3}$$

In the equation above, α_{rec} is the absorption efficiency of the absorber material, P_{inc} is the incident solar radiation reflected by the heliostat field determined in the heliostat field section. Note that the thermal efficiency of the solar receiver is defined as the fraction of absorbed thermal power $\dot{Q}_{abs}$ to the incident power P_{inc}.

$\dot{Q}_{loss}$ represents the combined losses due to conduction, convection, and thermal radiation, as expressed in Equation (4).

$$\dot{Q}_{loss} = A_{abs}\cdot\left(U_L\cdot\left(T_{int\_cav} - T_{amb}\right) + \alpha_{eff}.\sigma.\left(T^4_{int\_cav} - T^4_{amb}\right)\right) \tag{4}$$

A_{abs} is the absorber area, T_{amb} is the ambient temperature, U_L is the overall convective and conductive heat transfer coefficient, α_{eff} is the effective emissivity of the internal cavity receiver, and σ the Stefan-Boltzmann constant.

It is important to note that both U_L and α_{eff} are complex parameters that depend on the cavity receiver geometry and the experimental operating conditions. To ensure an acceptable accuracy calculation of the receiver performance, the proposed values for both U_L and α_{eff} as suggested by M.J. Santos et al [24] for the validation of their work have been employed. These were further confirmed by R.P. Merchan et al. [27] in a separate study.

The energy losses resulting from conduction, convection and radiation are calculated based on the average temperature of the internal cavity, T_{int_cav}, which is determined using Equation (5).

$$T_{int\_cav} = T_{air\_avg} + \frac{\dot{m}_{air}.cp_{air}.\left(T_{rec\_out} - T_{rec\_in}\right)}{A_{abs}.h_{int\_fc}} \tag{5}$$

T_{air_avg} is the average temperature of the air in the receiver $\left(\frac{T_{rec\_out}+T_{rec\_in}}{2}\right)$, T_{rec_in} is the air inlet temperature in the receiver equal to compressor outlet temperature T_{c_out}. h_{int_fc} is the heat transfer coefficient for internal flow forced convection.

The outlet temperature of the receiver (T_{rec_out}) is determined through an iterative calculation process by solving Equations (1) to (5). It is worth mentioning that the thermophysical properties of the air are calculated at average temperature using the REFPROP code.

Table 1
Characteristics of TAURUS 70S gas turbine. Please note that parameters marked with * were obtained from [42], those marked with ** were assumed for validation purposes, and those marked with *** were calculated.

Component	Parameter	Symbol	Value	Unit
Compressor	Air mass flow rate*	$\dot{m}_{air}$	25	kg/s
	Pressure ratio*	r_p	16:1	–
	Design speed*	n_c	15,200	rpm
	Isentropic efficiency**	η_c	73.5	%
	Specific heat ratio of air***	γ_{air}	1.38	–
Combustion chamber	Combustion efficiency**	η_{cc}	94	%
	Lower heating value of natural gas**	LHV	47.141	MJ/kg
	Natural gas mass flow rate***	$\dot{m}_{CH4}$	0.44	kg/s
	Air-fuel ratio***	AF	62.042	–
Turbine	Power*	$\dot{W}_t$	7.2	MW
	Recommended turbine inlet temperature*	T_{t_in}	1121	$^{\circ}C$
	Isentropic efficiency**	η_t	84	%
	Design speed*	n_t	6000–12000	rpm
	Specific heat ratio of gas**	γ_{gas}	1.325	–

3.3. Combustion chamber and turbine modeling

After leaving the solar receiver, where the air is preheated to T_{rec_out}, it enters the combustion chamber of the turbine section. The El Menia gas power plant utilizes the TAURUS 70S gas turbine model for electricity generation. This turbine operates on a simple Brayton cycle without a recuperator. The specifications of the turbine are detailed in Table 1.

The quantity of natural gas, $\dot{m}_{CH4}$, required for combustion is carefully controlled to ensure that the turbine inlet temperature, T_{t_in}, remains within the recommended limit set by the manufacturer ($T_{t\_in} \leq 1121^{\circ}C$). Additionally, the amount of natural gas is influenced by the value of T_{rec_out}, which varies daily and seasonally in response to the available DNI. Hence, higher values of T_{rec_out} result in reduced natural gas requirements.

To estimate the required amount of natural gas in the solar-gas hybrid mode of the power plant, an energy balance has been performed for the combustion chamber, leading to the development of Equation (6).

$$\dot{m}_{CH4} = \frac{\dot{m}_{air}.(H_{cc\_out} - H_{rec\_out})}{\eta_{cc}.LHV - H_{cc\_out}} \tag{6}$$

The H_{cc_out} represents the enthalpy of the combustion product mixture, which includes CO_2, O_2, H_2O, and N_2, and is evaluated at the recommended temperature of $T_{t\_in} \leq 1121^{\circ}C$ using Equation (7).

$$H_{cc\_out} = m_{CO2}H_{CO2} + m_{H2O}H_{H2O} + m_{O2}H_{O2} + m_{N2}H_{N2} \tag{7}$$

The mass fraction, m, for each combustion product is determined using a set of equations for combustion modeling, which are solved iteratively. The detailed model can be found in [43].

The net power output of the turbine is calculated using Equation (8).

$$\dot{W}_t = (\dot{m}_{air} + \dot{m}_{CH4}).(H_{t\_in} - H_{t\_out}) - \dot{m}_{air}.(H_{c\_out} - H_{c\_in}) \tag{8}$$

The enthalpy of the air at the compressor exit H_{c_out} is equal to the enthalpy of the air at the receiver entrance H_{rec_in}, while the enthalpy of the air at the compressor entrance H_{c_in} is evaluated at ambient temperature. Additionally, the enthalpy of gas mixture at the turbine entrance H_{t_in} is equal to the enthalpy of combustion products H_{cc_out}, while the enthalpy of exhaust gas at the turbine exit is calculated using a similar equation to Equation (7), replacing H_{cc_out} with H_{t_out} and evaluating the different combustion product enthalpies under the turbine outlet temperature using Equation (9).

$$T_{t\_out} = \frac{T_{t\_in}}{\left(1 - \eta_t\left(1 - \left(\frac{1}{r_p}\right)^{\frac{1-\gamma_{gas}}{\gamma_{gas}}}\right)\right)} \tag{9}$$

Two key parameters used to assess the performance of the solar-gas hybrid power plant are the overall thermal efficiency and the solar share factor, defined by Equations (10) and (11) [24].

$$\eta_{th} = \frac{\dot{W}_e}{\dot{m}_{CH4}LHV + P_{s\_field}} \tag{10}$$

The net electrical power produced, $\dot{W}_e$, is calculated assuming a generator and transmission efficiency of 98 %. The total solar radiation incident to the heliostat field, P_{s_field}, depends on the number of heliostats and their effective area, as well as the DNI, which varies hourly and seasonally.

$$f_s = \frac{\dot{Q}_{abs}}{\dot{Q}_{abs} + \eta_{cc}\dot{m}_{CH4}LHV} \tag{11}$$

After determining the required quantity of natural gas under the hybrid mode using Equation (6), we can calculate the annual volume of natural gas saved using Equation (12).

$$V_{s\_CH4} = V_{CH4\_con} - 3600.cf.\int_1^{8760} \dot{m}_{CH4}(t)dt \tag{12}$$

Where V_{CH4_con} represents the annual natural gas consumed by the original gas power plant without solar hybridization and $cf = 1.2412(m^3/kg)$ is used as the conversion factor to convert the mass of natural gas to volume. Furthermore, to estimate the amount of avoided CO_2 emissions, a factor of $2.649(\frac{kg_{CO2}}{kg_{naturalgas}})$ has been used as per the literature recommendation [44].

3.4. Economic model

The proposed modification to the El Menia gas power plant will require new investments related to the solar part, including the cost of heliostats, land, tower, and solar air receiver. As a result, the LCOE for this hybridization will differ from that of the original power plant. To estimate the minimum electricity sale price required for the hybrid power plant to be financially viable, we use Equation (13) [45].

$$LCOE = \frac{CRFZ_{inv} + Z_{O\&M}}{E_{ele}} \tag{13}$$

E_{ele} is the annual electrical energy generated by the hybrid power. The capital recovery factor, (CRF), is set to 9.88 % [45], and Z_{inv} represents the total investment for the hybrid power plant, which includes both the power block and solar tower systems along with their subsystems. The cost of each element of the entire hybrid system is determined using the formulation model reported by Spelling [46]. To account for inflation, as suggested in [27], the Marshall and Swift index has been utilized to adjust and update all equipment costs. $Z_{O\&M}$ denotes the annual operations and maintenance costs, which also incorporates the fuel cost, i.e., the natural gas consumption. For this study, the average price of natural gas in Algeria for 2023 was assumed, which was $1.1723 USD/MBtu$.

3.5. Heliostat field design and performance assessment

This study uses an in-house code to create a radial staggered heliostat field, previously detailed and validated by A. Belaid et al. [47] and T. Arrif et al. [48]. The code initially generates a full field, then removes inefficient heliostats, retaining only the more efficient northern half. As section 3.2 states, the solar receiver's incident thermal power P_{inc} equals the available solar radiation in the heliostat field times its optical

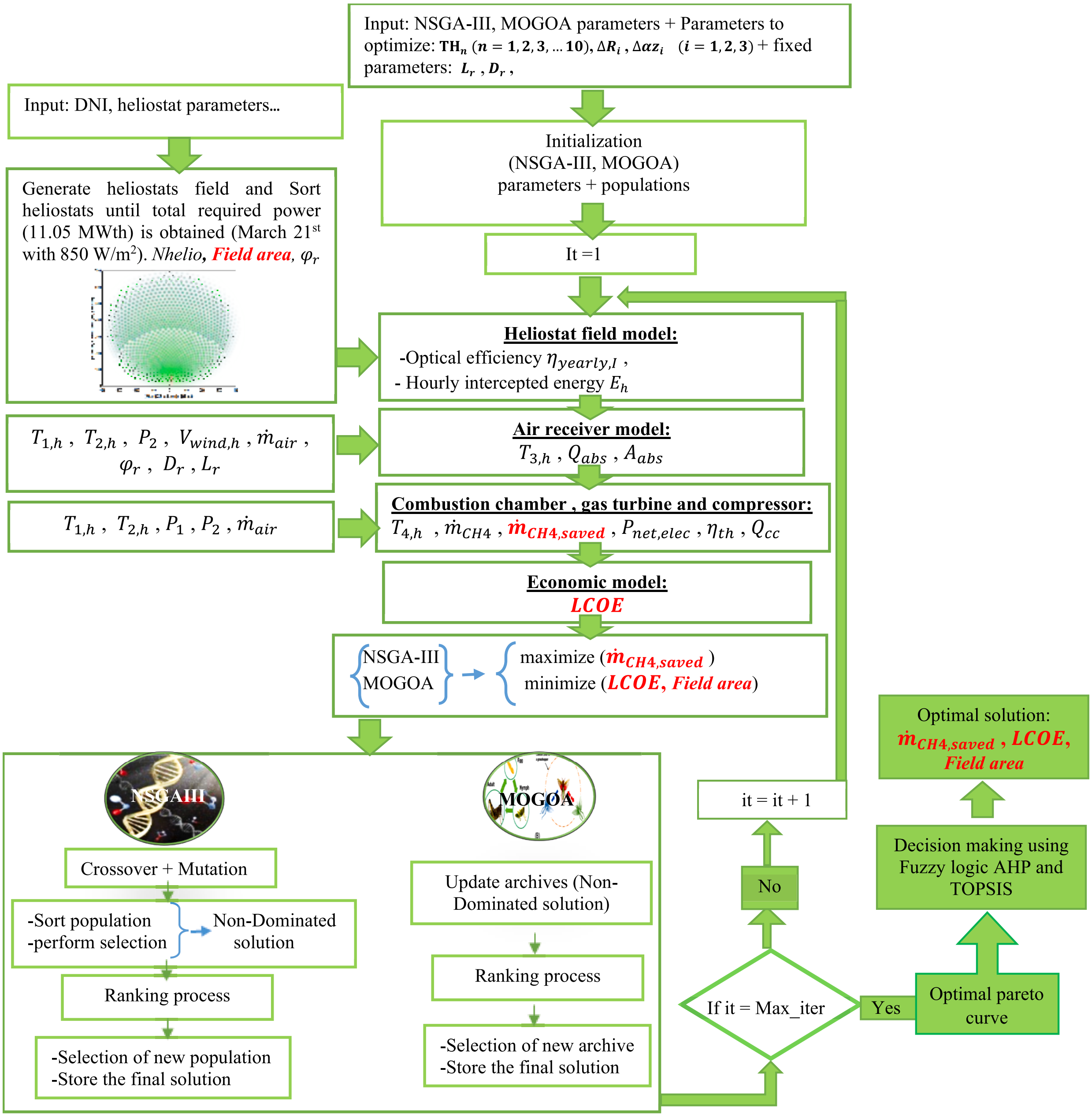

Fig. 4. Flow chart for NSGAIII and MOGOA Algorithms.

efficiency, as Equation (14) illustrates.

$$P_{inc} = \eta_{field} A_{ref\_field} DNI \tag{14}$$

A_{ref_field} denotes the total reflective area, which is equal to the number of heliostats, N_{hel}, multiplied by the area of a single heliostat, A_{sing}. The term DNI stands for the hourly direct normal irradiance, as presented in Fig. 2.

The land footprint of the new hybrid power plant has been assessed using a factor called Land Use Factor (*LUF*). This factor is determined using Equation (15).

$$LUF(\%) = 100 \bullet \frac{A_{hf} + A_{pp}}{A_{tot}} \tag{15}$$

A_{hf}, A_{pp}, and A_{tot} represent the heliostat land area, the area of the original gas power plant before modification, and the total land area owned by the company, respectively. A_{pp} and A_{tot} are estimated at 10*ha* and 150*ha*, respectively. A_{hf}, which varies with the installed solar power, is a key target for optimization.

4. Optimization methodology

To optimize hybrid power systems for techno-economic and environmental efficiency, three objectives are prioritized: minimizing LCOE and land area usage (A_{field}), and maximizing natural gas savings (V_{s_CH4}). The optimal design balances these criteria. The study employs two multi-objective optimization methods: the NSGA-III [49,50] and the MOGOA for multi-objectives [51]. This marks MOGOA's first use in optimizing hybrid solar gas power plants. Both algorithms generate diverse solutions along the Pareto front, offering decision-makers various trade-off options.

The general optimization flowchart for the two algorithms used in this study is depicted in Fig. 4 and can be summarized as follows:

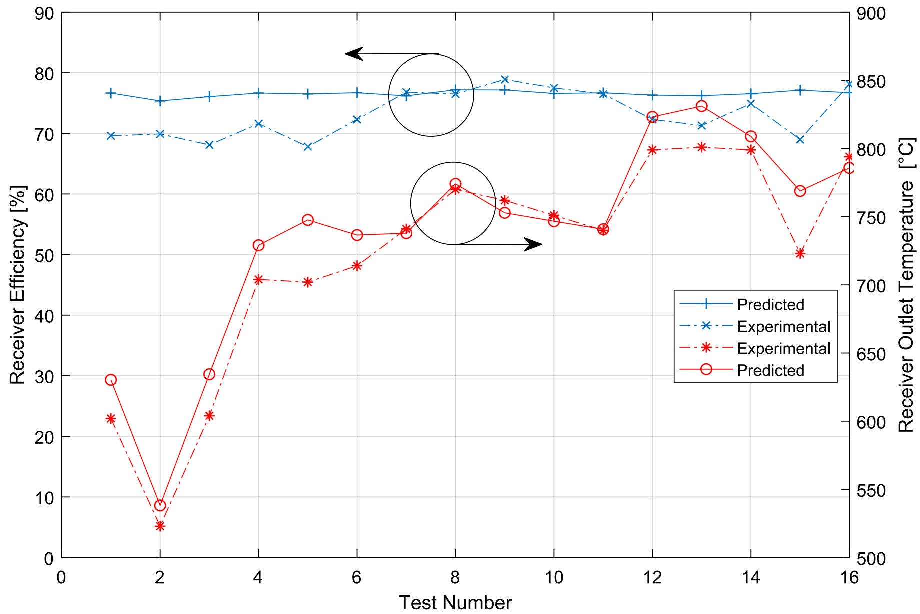

Fig. 5. Validation of the thermal model for pressurized air receiver. The test numbers correspond to the experimental tests and their respective validation results.

1. The optimization algorithm (NSGA III, MOGOA) assigns random values to ΔR_i, $\Delta \alpha z_i$, and TH_n in the defined range.
2. A large heliostat number, greater than the expected size of the field, is generated (1500 heliostats were generated).
3. The security distances between the adjacent heliostats are simultaneously checked to ensure there is no collision between adjacent heliostats.
4. All the candidate heliostats are evaluated in the absence of shading and blocking at noon on March 21st under DNI value of 850 W/m^2. The sun position is calculated according to the hybrid power plant's location (El-Golea, Algeria, at noon March 21st).
5. This step involves sorting the candidate heliostats in descending order based on their individual efficiencies. The number of heliostats is then counted until the total thermal power incident on the solar air receiver reaches 11.5 MWth. This step determines the number of heliostats and, consequently, the field area, which is the first objective function.
6. The weighted efficiency of the resulting heliostat field, along with its associated tower height, will be evaluated on a yearly basis, considering the shading and blocking efficiencies.
7. Next, the air receiver, combustion chamber, gas turbine and economic analysis models are applied to calculate the natural gas volume saved V_{s_CH4}, and $LCOE$ for the corresponding heliostat field. This step allows us to obtain the second and third objective functions.
8. Finally, the NSGA-III and MOGOA algorithms employ their respective criteria to obtain the final optimized solution.
9. Up to this step, a complete iteration is performed, and the entire process is repeated starting from Step 1 until the maximum predefined iteration is achieved. By doing so, the two optimizers will generate optimal Pareto curves, showcasing the different trade-offs among the objectives and providing a range of efficient solutions for the hybrid solar gas power plant design.

The optimization in this study is conducted over 12 representative days of the year, selected for each month's distinct DNI, temperature, and wind speed, significantly reducing computational time. This method is inspired by previous research such as S.M. Besarati, D. Yogi Goswami [51], and P. Piroozmand, M. Boroushaki [52]. The final design is chosen based on expert priorities using Fuzzy logic AHP and TOPSIS decision methods. After selection, the hybrid plant's yearly performance is recalculated with daily averages, providing a thorough evaluation of its efficiency and alignment with government energy policies.

Table 2
Parameters and characteristics of the proposed air receiver for the present application compared to SOLUGAS project's receiver. All of the parameters indicated in the table for SOLUGAS project's receiver are taken from [21], except that marked by (*) has been calculated. The assumed values for U_L and α_{eff} taken from [24].

Parameters	Unite	Pressurized air receiver design for the current application	SOLUGAS project's receiver
Thermal power	MW_{th}	11.5	3.2
Design receiver outlet temperature	$^{\circ}C$	800	800
Mass flow rate	kg/s	25	5.7
Working pressure	bar	16	9
Absorber area	m^2	193.5	~ 60
Aperture area	m^2	~12.6	~ 6
Absorber radiated length	m	5	5
Receiver diameter	m	4	2.75
Tube inner diameter	mm	19.6	19.6
Tube thickness	mm	1.4	1.4
Number of panels	–	22	10
Number of tubes per panel	–	25	17
Maximum air velocity	m/s	25.35	26.2*
Conduction and convective heat transfer coefficient U_L	$Wm^2.K$	5	5
Effective emissivity α_{eff}	–	0.1	0.1

5. Results and discussion

This section has three parts: validating the mathematical models, comparing optimization results from NSGA-III and MOGOA, and analyzing the El Menia plant's hybrid mode's techno-economic performance. The analysis will highlight the system's efficiency and economic potential for improvement and implementation.

5.1. Model validation

The accuracy of the thermal model for assessing the receiver's performance was checked by comparing its predictions with experimental

Table 3
Validation results for combustion chamber and turbine modeling.

	Inlet turbine temperature ($^{\circ}C$)	Outlet turbine temperature ($^{\circ}C$)	Turbine power (kW)	Turbine efficiency (%)
Experimental [42]	1121	488	7236	34
Present model	1119.8	493	7238.1	34.89
Deviation (%)	−0.1070	1.0246	0.03	2.617

Note that the turbine inlet temperature, and to some extent the combustion chamber temperature, greatly depends on the amount of natural gas injected and the efficiency of the combustion chamber. Therefore, accurately predicting the mass flow rate of the natural gas leads to a precise determination of the turbine inlet temperature. Based on the data presented in Table 3, it can be confirmed that the developed model accurately predicts the mass flow rate of the natural gas and various turbine parameters.

results from R. Korzynietz et al. [21], focusing on outlet temperature and efficiency of the receiver.

Fig. 5 shows that the predicted data closely match experimental results, with a mean deviation of 5.57% for receiver efficiency and 2.76% for outlet temperature. This indicates the thermal model's accuracy, making it reliable for use. Additionally, Table 2 compares parameters of the proposed receiver design with the SOLUGAS project's receiver.

The design of the solar receiver, including the number of tubes and panels, ensures air velocity doesn't exceed 26m/s, and the outlet air temperature stays below 800$^{\circ}C$ to align with the material tolerance of typical solar air receivers.

Model accuracy for predicting natural gas requirements was validated by comparing model data with actual THAURUS 70S [42] turbine field data, detailed in Table 3.

5.2. Output of multi-objective optimization of both NSGA-III and MOGOA

To address the stochastic nature of the optimization methods, multiple runs have been conducted for each method. Specifically, each optimization method was executed 6 times, with the number of iterations set to 100 and the population size to 40 for each run. The results for the three chosen objectives, and heliostat field performance are presented in Fig. 6 and Fig. 7, respectively.

Fig. 6 shows that NSGA-III achieved a lower average LCOE (89.87USD/MWh) compared to MOGOA (90.24USD/MWh). However, MOGOA surpassed NSGA-III in annual natural gas savings, with MOGOA's top 240 solutions averaging 2.381Mm^3, slightly higher than NSGA-III's 2.376Mm^3.

Fig. 7 reveals that NSGA-III optimizes heliostat fields more efficiently than MOGOA, resulting in smaller areas (9.46ha for NSGA-III vs. 10.83ha for MOGOA) and slightly higher optical efficiency (74.32% for NSGA-III vs. 74.24% for MOGOA). NSGA-III's smaller heliostat fields contribute to its lower LCOE, while MOGOA's larger fields yield better annual natural gas savings due to increased solar radiation capture, however with a higher LCOE. Thus, it's evident that the two methods prioritize differently: NSGA-III emphasizes minimizing LCOE and heliostat field area, while MOGOA prioritizes maximizing gas savings.

Choosing the best design for a hybrid power plant is complex, involving a balance between LCOE, gas savings, and heliostat field size. To address this, the study uses the hybrid Fuzzy AHP-TOPSIS method for decision making. This method incorporates expert-defined scenarios and weights for each objective (illustrated in Figs. 8 and 9, detailed in Table 5, with priorities from Table 4). The linguistic terms for these priorities are based on triangular fuzzy numbers (referenced in [52]).

This multi-criteria decision-making approach aids in identifying the most suitable design point, considering the trade-offs between the three key objectives.

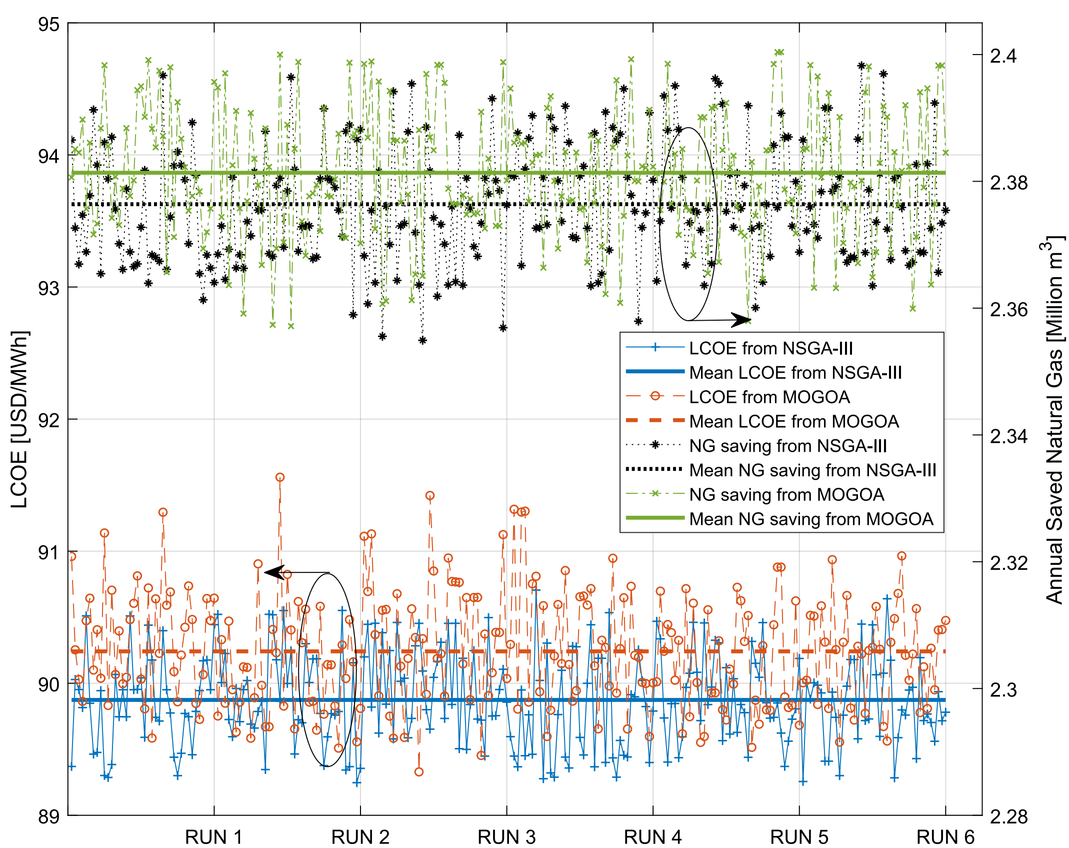

Fig. 6. LCOE and annual saved NG obtained from NSGA-III and MOGOA.

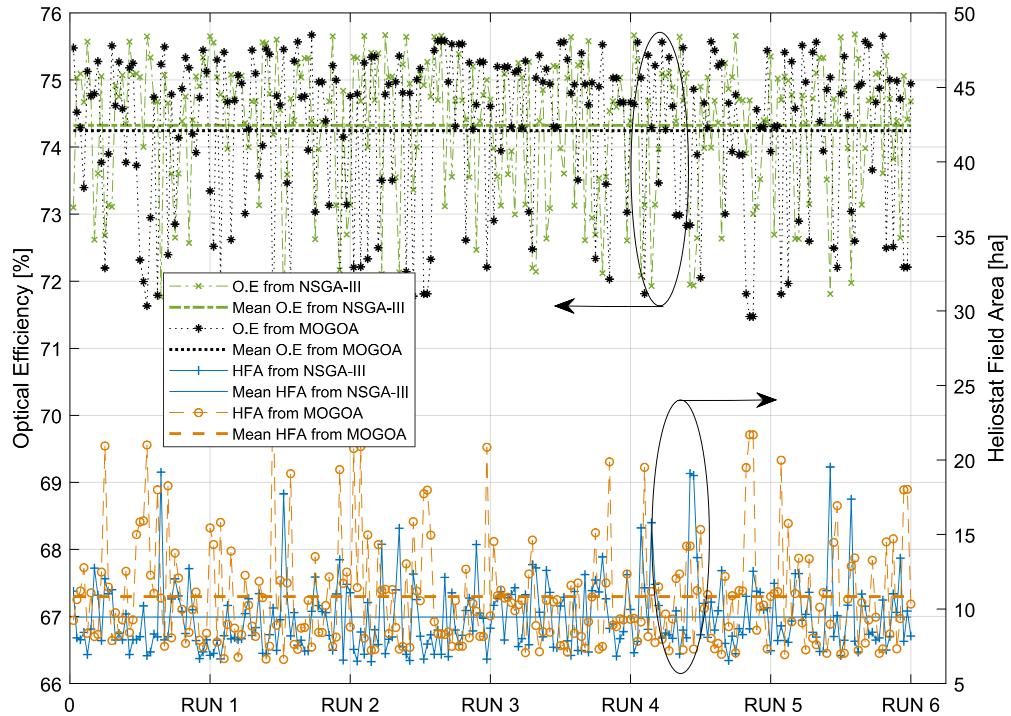

Fig. 7. Optical Efficiency (OE) and Heliostat field Area (HFA) obtained from NSGA-III and MOGOA.

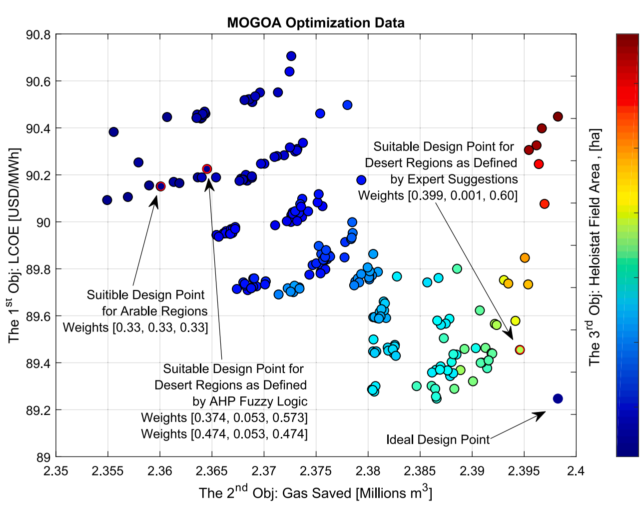

Fig. 8. Selection of design points using the Fuzzy AHP-TOPSIS method and expert opinion, based on data optimized by the NSGA-III method.

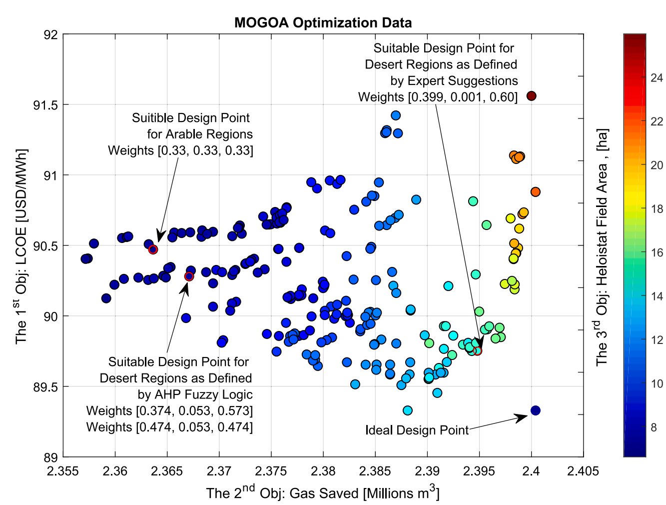

Fig. 9. Selection of design points using the Fuzzy AHP-TOPSIS method and expert opinion, based on data optimized by the MOGOA method.

The ideal design points in Figs. 8 and 9, representing minimal LCOE and LUF with maximum natural gas savings, are unfeasible for implementation. They serve as reference points in the TOPSIS algorithm, which also incorporates weight outputs from the Fuzzy Logic AHP method to select various design points shown in these figures.

Figs. 8 and 9 show a clear link between annual natural gas savings and the size of the heliostat field, regardless of whether NSGA-III or MOGOA optimization methods are used. The LCOE is influenced not only by land area but also by tower cost. Smaller heliostat fields require taller towers, while larger fields need shorter ones. Further LCOE analysis will be presented later.

NSGA-III tends to produce fewer solutions with larger heliostat fields, as seen in its sparser scatter plot, in contrast to MOGOA, which offers more uniform distribution with numerous high-field area solutions. This suggests NSGA-III may prioritize smaller heliostat fields compared to MOGOA.

Both methods yield unique optimal points based on objective function weights. Three implementation scenarios aligning with government priorities emerge. In arable regions, all objectives receive equal priority. In desert regions, land importance diminishes. Details can be found in Table 5.

The scenarios for arable regions, across both optimization methods, closely align with the ideal point in terms of land area. However, the suggested design points for desert regions are not as impressive in terms of LCOE, and annual natural gas savings. For instance, the ideal design point for NSGA-III has outputs of $2.398 Mm^3$, $89.25 USD/MWh$, and $6.468 ha$, whereas the outputs for the desert regions' weights yield similar scenarios of $2.364 Mm^3$, $90.22 USD/MWh$, and $6.647 ha$. While the land area is closely aligned with the ideal point, the LCOE, and annual natural gas savings fall short. Comparable observations apply to

Table 4
Expert-derived pairwise comparisons using triangular fuzzy numbers.

Objectives	Gas saving	LCOE	Land Area	Consistency Ratio (RC)	Weights	
Fuzzy AHP case 1	Gas saving	(1, 1, 1)	(1, 1, 1)	(1, 1, 1)	0.00	0.333
	LCOE	(1, 1, 1)	(1, 1, 1)	(1, 1, 1)		0.333
	Land Area	(1, 1, 1)	(1, 1, 1)	(1, 1, 1)		0.333
Fuzzy AHP case 2	Gas saving	(1, 1, 1)	(1, 1, 1)	(9, 9, 9)	0.00	0.474
	LCOE	(1, 1, 1)	(1, 1, 1)	(9, 9, 9)		0.474
	Land Area	(1/9, 1/9, 1/9)	(1/9, 1/9, 1/9)	(1, 1, 1)		0.053
Fuzzy AHP case 3	Gas saving	(1, 1, 1)	(1, 2, 3)	(9, 9, 9)	0.06	0.573
	LCOE	(1/3, 1/2, 1/1)	(1, 1, 1)	(7, 8, 9)		0.374
	Land Area	(1/9, 1/9, 1/9)	(1/9, 1/8, 1/7)	(1, 1, 1)		0.053

MOGOA, the LCOE and annual natural gas saving values remain less than ideal.

To further emphasize the scenarios with higher annual natural gas savings, the priority given to the heliostat field area should be decreased. However, the 9-scale priority system used by the Fuzzy AHP decision-making method does not permit weight values below 0.053 for the heliostat field area. Expert recommendations led to modifications in Fuzzy AHP Case 3 for the desert region hybrid power plant, setting expert-adjusted weights at 0.399 for LCOE, 0.001 for land area, and 0.600 for natural gas savings.

The scenarios resulting from Expert Opinion Case 4 show particularly promising results in terms of LCOE and annual natural gas savings, especially with the NSGA-III method. Notably, there's a reduction of 0.85% in LCOE compared to Fuzzy AHP Case 3. This reduction is largely due to the decrease in tower height from 75*m* to 35*m*, which subsequently lowers the tower's cost from 4.24 million USD to 2.98 million USD. While there is an increase in land area in Expert Opinion Case 4, the associated cost rise is marginal, increasing from 10.1 million USD to 10.8 million USD, thus not significantly affecting the LCOE. On the other hand, there's a noteworthy increment of approximately 1.31% in annual natural gas saving when juxtaposed with Fuzzy AHP Case 3. While both optimization methods show equal annual natural gas savings at 2.395Mm^3, NSGA-III exhibits a more favorable LCOE and land area, as presented in Table 6.

Given the analysis of each optimization method and the results from the decision-making process, the Expert Opinion Case 4 scenario from the NSGA-III method has been selected as the design proposal for the upcoming hybrid solar gas power plant proposed for Sonalgas Company.

5.3. *Annual performance of the hybrid solar tower gas power plant under the selected design point*

The heliostat field from NSGA-III has a slightly lower environmental impact compared to MOGOA's field. Further characteristics of the selected design for the heliostat field are presented in Table 6.

Fig. 10 shows the yearly temperatures variation of different subsystems in the hybrid power plant. The air receiver outlet temperature usually stayed below 800 °C, the absorber material's limit. However, it exceeded 800 °C briefly in late August and early autumn. This is not critical, as the control system can defocus heliostats to reduce radiation. Heliostat defocusing was required for only 64 h, about 1.8 % of the yearly sunny hours.

Table 6
Heliostat field characteristics under the selected design point for NSGA-III.

Parameters	Value	Unit
Land area	13.5	*ha*
Heliostat number	350	–
Heliostat area	50	m^2
Minimum heliostats separation distance	10.07	*m*
First row distance from tower	10	*m*
Mirror reflectivity	0.9	
Blocking and shadowing efficiency	98.2	%
Attenuation efficiency	96.5	%
Cos efficiency	81.5	%
Field optical efficiency	72	%
Sun deviation	2.51	*mrad*
Heliostat optical error	2.9	*mrad*
Tower height	35	*m*
Receiver diameter	4	*m*
Concentration ratio	1389	–

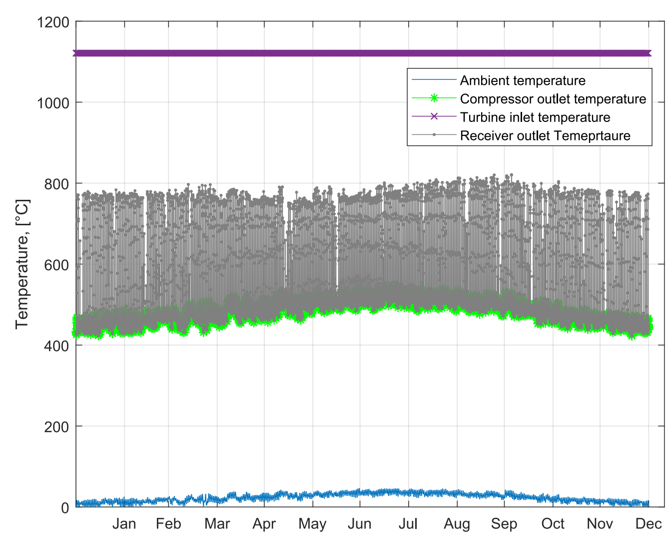

Fig. 10. Hourly temperature variation of the air from ambient to the receiver outlet, corresponding to the selected design point for NSGA-III.

Table 5
Design point selection for NSGA-III and MOGOA based on Fuzzy Logic AHP and expert opinion for the weights determination and TOPSIS for decision-making.

	Weights			LCOE (USD/MWh_e)		Land Area (ha)		Gas Saved (Mm^3)	
	W_{LCOE}	$W_{LandArea}$	$W_{GasSaved}$	NSGA-III	MOGOA	NSGA-III	MOGOA	NSGA-III	MOGOA
Fuzzy AHP case 1	0.333	0.333	0.333	90.15	90.47	6.541	6.671	2.360	2.364
Fuzzy AHP case 2	0.474	0.053	0.474	90.22	90.28	6.647	7.028	2.364	2.367
Fuzzy AHP case 3	0.374	0.053	0.573	90.22	90.28	6.647	7.028	2.364	2.367
Expert opinion case 4	0.399	0.001	0.600	89.45	89.75	13.5	14.33	2.395	2.395

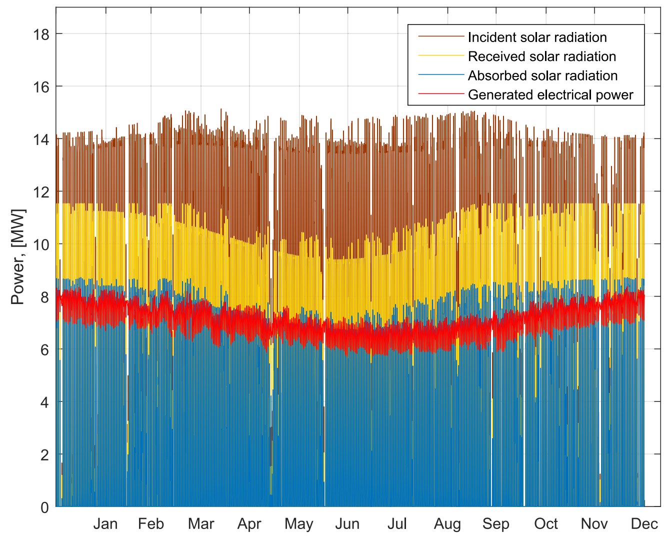

Fig. 11. Annual hourly variation in available powers at the hybrid power plant. Data is based on the selected design point for NSGA-III.

Fig. 11 shows the yearly hourly variation in available powers at the hybrid power plant, and Fig. 12 focusing on noon values. Annually, the heliostat field gets about 13.8 MW of incident solar power, with 10.4 MW reflected to the air thermal receiver and 7.65 MW absorbed as thermal power. Peak irradiance occurs in spring and autumn. Winter sees reduced solar radiation due to low sun elevation, while summer's decrease is due to airborne dust from sandstorms. In addition, the summer decrease in reflected solar radiation is mainly due to the cosine effect and lower attenuation factor. Conversely, the drop in electrical power generation is caused by the compressor using more mechanical power to pressurize hot summer air. Note that, the sharp drops in Fig. 12 indicate cloudy days or sandstorms.

The annual energy performance of the hybrid solar gas power plant are presented in Table 7. Specifically, the plant receives an annual incident solar energy of 38.3GWh, of which the heliostat field reflects 27.5GWh. The net thermal energy absorbed by the air receiver amounts to 19.6GWh. Thus, the optical performance of the designed heliostat field and the absorbing efficiency of the air thermal receiver are 72% and 71.3%, respectively. The required combustion energy from natural gas has been found to be 158GWh. It's worth noting that while under 100 % natural gas operation this energy amounts to 183.6GWh.

Fig. 13 illustrates the annual variations in heat input from natural gas combustion for both the hybrid mode and the original mode without solar input at noon time. The heat input from the combustion chamber is influenced by both the ambient temperature and the heat absorbed by the air thermal receiver, which preheats the air.

Consequently, there is a corresponding reduction in the mass flow rate of natural gas consumption, as confirmed by Fig. 14. A closer examination of the natural gas consumption curve for a 24-hour period on March 21st reveals the mass flow rate of natural gas during daylight at noon is almost halved in the hybrid mode, dropping to 787kg/h compared to 1570kg/h in the original mode.

The hourly mass flow rates depicted in Fig. 14 were accumulated and subsequently converted into volume, a unit more frequently used by financial departments and natural gas trading entities. The findings are displayed in Fig. 15. It is pertinent to highlight that the reduced

Table 7
Annual energetic performance of the hybrid power plant.

Parameters	Value	Unit
Available solar energy	38.3	GWh_{th}
Reflected solar energy	27.5	GWh_{th}
Absorbed solar energy	19.6	GWh_{th}
Combustion energy	158	GWh_{th}
Electrical energy	62	GWh_{th}
Power plant efficiency	31.74	%
Solar share	11.64	%

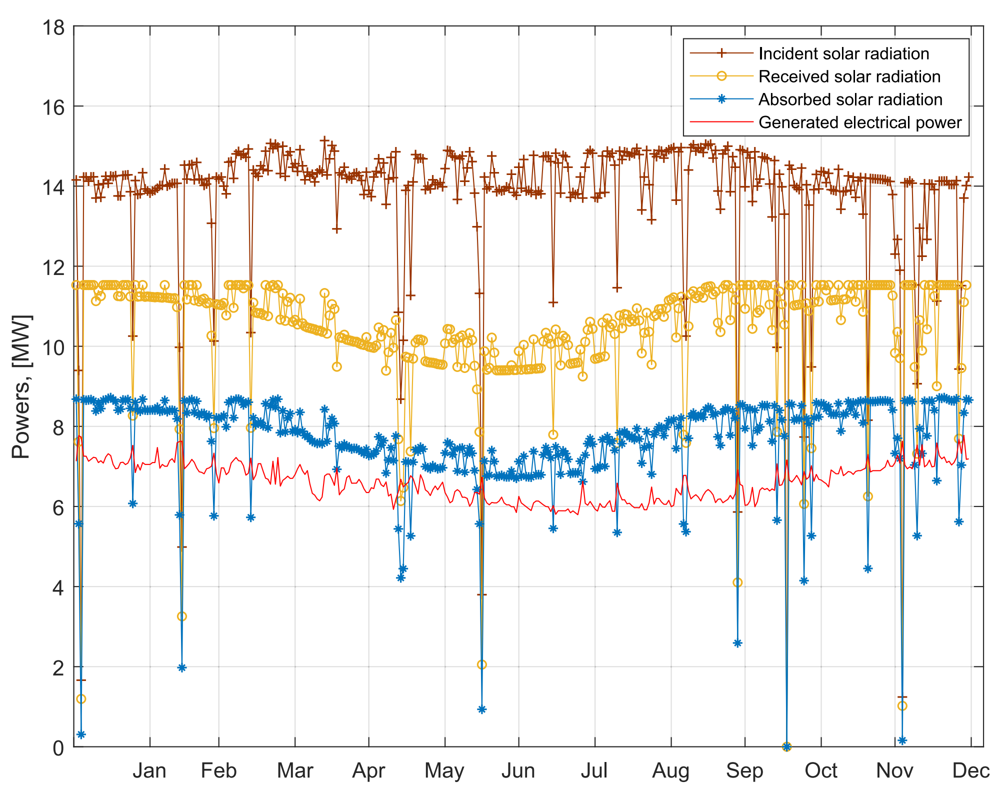

Fig. 12. Annual variation in available powers from the hybrid power plant at noon. Data is based on the selected design point for NSGA-III.

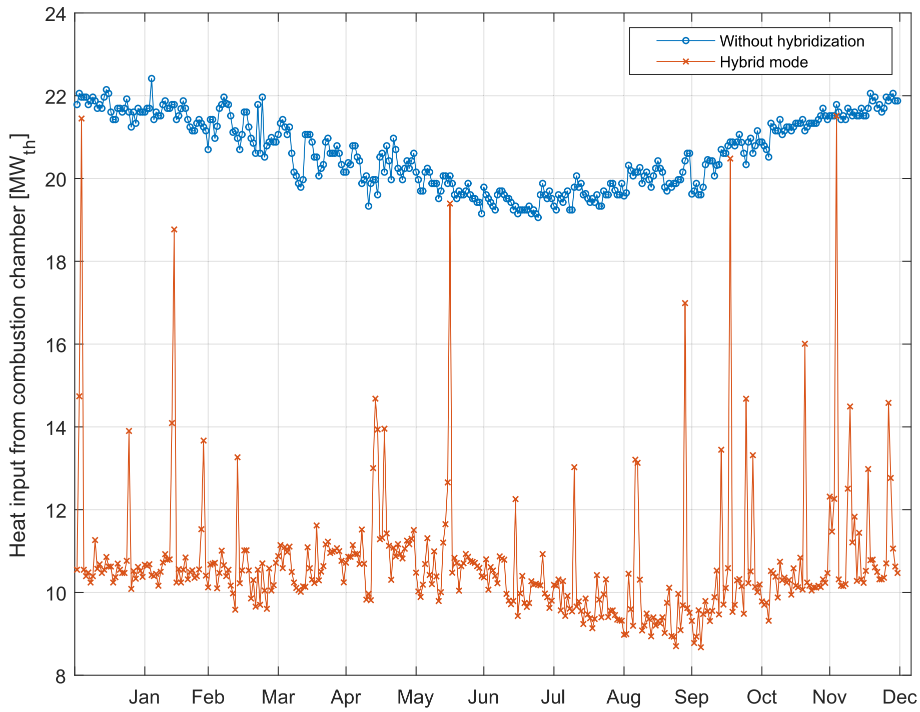

Fig. 13. Annual hourly heat input from the combustion chamber, comparing the hybrid mode based on the selected design point for NSGA-III, with the original mode.

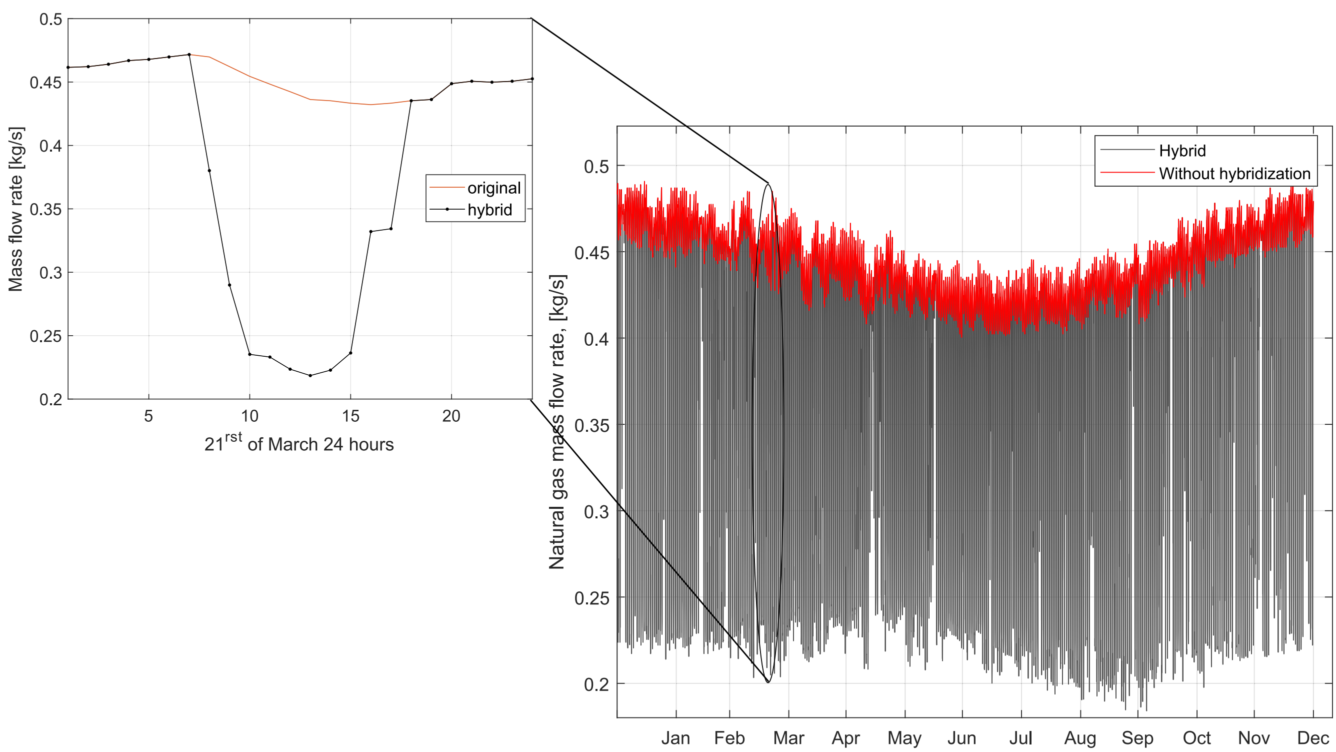

Fig. 14. Hourly variation of natural gas mass flow over a year, comparing the original mode with the hybrid mode.

consumption recorded in February is attributable to the fewer operating hours characteristic of this month. On the other hand, the months of March through August register the highest savings in natural gas volume, peaking at 0.23Mm^3 in April. Conversely, the smallest savings, amounting to 0.156Mm^3, are seen in December. Based on the insights provided in Fig. 15 the most suitable months to schedule maintenance operations for the hybrid power plant are either January or December.

In summary, the power plant's annual natural gas consumption stands at 17.41Mm^3, amounting to an annual cost of 1.88 million USD. However, by incorporating the solar tower technology for hybridization, this volume drops by 13.8 % to 15Mm^3, thereby ensuring an impressive annual saving of 2.41Mm^3 in natural gas in terms of volume and

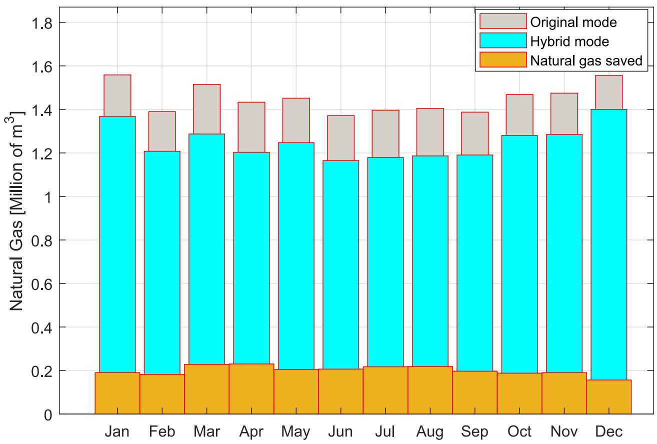

Fig. 15. Comparison of the annual natural gas consumption by the power plant under 100% fossil fuel operation and solar-hybridized mode, and the monthly volume of natural gas saved through hybridization.

approximately ∼ 260,000 USD in financial terms. Moreover, this quantity of natural gas equates to the yearly average consumption of approximately 3600 Algerian households.

Integrating a gas power plant with solar tower technology reduces natural gas use and carbon footprint but requires more investment, as shown in Fig. 16. The heliostat field represents 44.8 % of total costs, while the thermal receiver and tower are 19.1% and 1 2.4%, respectively. This raises the LCOE to $89.5USD/MWh$ (see Table 8). While the resulting LCOE has been found in line with values in the literature [35,54], but there are concerns about the heliostat field cost estimation used in the model reported in ref. [28]. The model suggests a heliostat cost of $200USD/m^2$, higher than recent estimates [53 54].

Consequently, the resulting LCOE for the hybrid power plant may not reflect its actual energy cost, complicating decision-making for local policymakers and stakeholders. To attain a more accurate LCOE, the costs of CSP components, especially heliostats and tower, were reassessed. A lower heliostat cost of $140USD/m^2$ [53] and a land acquisition cost of $1USD/m^2$ in the desert region were considered. Additionally, while the air thermal receiver might require imports, local manufacturing of the heliostat field and tower can reduce costs by at least 15 % as suggested by the expert, leveraging native materials, energy, and labor, and benefiting from lower local expenses compared to European standards.

Following these adjustments, the revised costs for the heliostat field and tower stand at 6.9 million USD and 2.53 million USD, respectively. Consequently, the recalculated LCOE for the hybrid solar gas power plant now stands at $78USD/MWh$. With the refined parameters to reassess the CSP components' costs, it is reasonable to conclude that this updated LCOE is much more accurate. If any margin of error remains, it is more likely the figure is an overestimation rather than an underestimation.

Furthermore, the recalculated LCOE for the hybrid solar gas power plant has proven to be more competitive compared to the global weighted average LCOE in 2022 for offshore wind and Concentrated Solar Power, which were $81USD/MWh$ and $118USD/MWh$, respectively [55].

The 13.8 % emissions reduction and LCOE increase to 78 USD/MWh reflect a deliberate trade-off: integrating solar energy into an existing gas turbine to reduce fossil fuel consumption while maintaining dispatchability. Unlike standalone CSP or wind offshore, which offer zero emissions but are intermittent, the present hybrid system provides continuous power, which is a critical advantage over intermittent renewables. This approach leverages existing infrastructure, facilitating a gradual transition to low-carbon energy in regions reliant on natural gas.

Introducing recuperative turbine or combined cycle indeed offers greater efficiency potential; however, it involves entirely new investment decisions, including full turbine replacement or new plant construction. Such changes would deviate from the study's original objective of offering a practical retrofit solution.

An environmental assessment for the modified gas power plant shows an increase in land use from 6.67% to 15.67%. However, in desert or remote areas, like in this study, where land isn't crucial for agriculture or ecosystems, the impact of hybrid power plants is considered acceptable and not environmentally destructive.

In terms of carbon dioxide emissions, the gas power plant releases $37.15kt$ of CO_2 annually, and after hybridization, this amount decreases to $32kt$, marking an annual emission avoidance of $5.15kt$ of CO_2. This equates to a reduction rate of approximately $81.6gCO_2/kWh$ (or $715tCO_2$ per hybrid megawatt-electric installed). Moreover, if a carbon

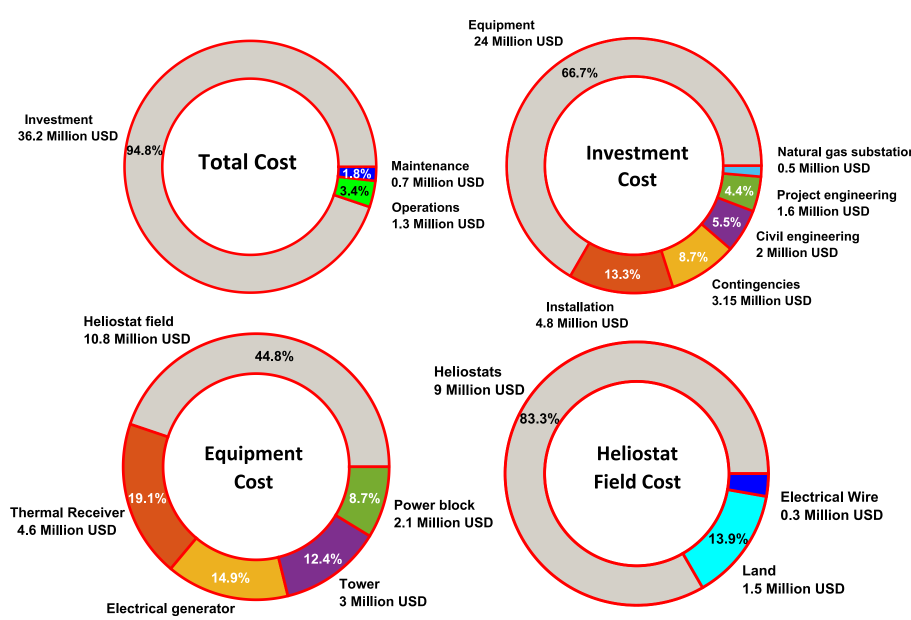

Fig. 16. Cost breakdown analysis for the hybrid power plant, corresponding to the selected design point from NSGA-III. Note that, the operation and maintenance costs are expressed in annual terms.

Table 8
Economic performance and environmental impact of the power plant with and without hybridization.

Parameters	Original mode*	Hybridized mode		Difference	
Annual natural gas consumption (Million m^3)	17.41	15		−2.41	
Yearly natural gas bill based on exporting price (Million USD)	1.88	1.62		−0.26	
LCOE (USD/MWh)	38.83	89.5	78**	+ 50.5	+ 39
CO_2 Emissions (kt)	37.15	32		−5.15	
Carbon Tax (USD)	668,700	576,000		92,700	
LUF (%)	6.67	15.67		+ 9	

*100% Natural gas mode.
**Estimation based on the scenario in which the heliostat field and tower are planned to be manufactured locally.

tax or Emission Trading Scheme similar to the one in Spain, priced at 18 USD per ton of CO_2 [56], is implemented, could yield annual savings of 92,700 USD in carbon emission taxes.

While the case study presented in this paper is located in Algeria, the findings have broader implications, particularly for regions with high concentrated solar potential and a substantial share of electricity production from natural gas. Consequently, an effort has been made to explore the potential impact of this study in the MENA region. According to Ember Electricity Data Explorer [57], the MENA region's electricity production from natural gas in 2022 amounted to 12 TWh. With the carbon intensity of natural gas-generated electricity around 490 gCO_2/kWh [58], this translates to approximately 586 million tonnes of CO_2 emissions. Therefore, implementing the concepts and findings from this study in the MENA region could potentially reduce CO_2 emissions by as much as 96 million tonnes.

6. Conclusion

This study has extensively investigated the hybridization of a gas power plant with solar tower technology, focusing on optimization, economic assessment, and environmental impact. The research findings and outcomes can be summarized as follows:

1. Multi-objective optimization was conducted using two distinct methods, NSGA-III and MOGOA. NSGA-III demonstrated superiority in achieving a lower LCOE, while MOGOA excelled in delivering higher annual natural gas savings. The selection between these methods ultimately depends on the primary focus, whether it be cost reduction or gas savings.
2. The decision-making process employed a Fuzzy-AHP coupled with TOPSIS to identify the optimal design point among various scenarios. The chosen scenario, recommended by experts, prioritized gas savings while maintaining competitive LCOE and LUF.
3. The hybridization led to a notable reduction in natural gas consumption, amounting to 13.8%. This translated to an annual savings of 2.41Mm^3 in volume and approximately 260,000 USD in financial terms. Remarkably, this volume of saved natural gas equated to the yearly average consumption of around 3600 Algerian households.
4. A comprehensive cost breakdown and LCOE analysis revealed that, while introducing CSP components initially increased investment costs, a reevaluation of cost parameters resulted in a significantly more competitive LCOE of 78USD/MWh. This positions the hybrid solar-gas power plant as a promising and economically viable addition to Algeria's energy landscape, especially considering recent pricing benchmarks.
5. In terms of environmental impact, the LUF increased to 15.67 %, but considering the desert location and minimal impact on agriculture, the environmental impact is acceptable. Furthermore, carbon dioxide emissions could be reduced by 81.6gCO_2/kWh (or 715tCO_2/MWe) annually contributing positively to sustainability goals, and could lead to an annual savings of 92,700 USD in relation to the taxes imposed on carbon emissions.
6. Applying the concepts and findings of this study to the MENA region, which heavily relies on natural gas for electricity, could potentially reduce CO_2 emissions by up to 96 million tonnes.

Future work could explore the integration of a recuperative turbine and thermal energy storage to enhance system flexibility and reduce natural gas consumption. This approach could potentially increase the solar share beyond the current 11.64 % and yielding additional emissions reductions.

In summary, while the hybrid concentrated solar gas power plant demands a substantial initial investment, there is potential for cost reductions through future optimization studies. Notably, this hybrid plant could stand out for its conservation of fossil fuel resources and its capability to reduce pollutant emissions. Such attributes highlight its value as a pivotal low-carbon technology in the energy transition journey, a fundamental commitment not only in Algeria but also in numerous fossil fuel-consuming countries for the upcoming decade.

CRediT authorship contribution statement

Samir Hassani: Writing – original draft, Visualization, Validation, Supervision, Software, Methodology, Investigation, Formal analysis, Conceptualization. **Toufik Arrif:** Visualization, Validation, Software, Methodology, Formal analysis. **Mawloud Guermoui:** Methodology, Formal analysis. **Noureddine Yassaa:** Writing – review & editing, Validation, Methodology. **Abdelfetah Belaid:** Validation, Software, Methodology. **Rosa Pilar Merchán Corral:** Writing – review & editing, Validation, Methodology. **Badraddine Bezza:** Software. **Robert A. Taylor:** Writing – review & editing. **Saad Mekhilef:** Writing – review & editing.

Declaration of competing interest

The authors declare that they have no known competing financial interests or personal relationships that could have appeared to influence the work reported in this paper.

Acknowledgement

This study is conducted in collaboration with the Sonelgaz Company, a state-owned utility in charge of electricity and natural gas distribution in Algeria, as well as promoting renewable energy applications in the Algerian desert. We extend our gratitude to the DGRSDT and Sonelgaz Company for their invaluable support in conducting this study.

Data availability

All data supporting the findings of this study are provided within the article.

References

[1] WRI. Reckoning and Recovery: Working toward a More Equitable and Sustainable Future. WRI Annual Report Washington, DC 20002, USA2021.
[2] BP statistical review of world energy 2024. Accessed February 2025.
[3] W.-M. Małgorzata, F. Nicolas, D. Jones, Global electricity review 2024, Ember (2024).

[4] IEA(2022). Global Energy Review: CO2 Emissions in 2021. IEA, Paris https://www.iea.org/reports/global-energy-review-co2-emissions-in-2021-2.
[5] T. Lei, D. Guan, Y. Shan, B. Zheng, X. Liang, J. Meng, et al., Adaptive CO2 emissions mitigation strategies of global oil refineries in all age groups, One Earth 4 (2021) 1114–1126.
[6] IRENA(2022). World Energy Transitions Outlook 2022: 1.5°C Pathway International Renewable Energy Agency, Abu Dhabi.
[7] B.A.A. Yousef, A.A. Hachicha, I. Rodriguez, M.A. Abdelkareem, A. Inyaat, Perspective on integration of concentrated solar power plants, International Journal of Low-Carbon Technologies. 16 (2021) 1098–1125.
[8] O. Achkari, A. El Fadar, Latest developments on TES and CSP technologies – Energy and environmental issues, applications and research trends, Appl. Therm. Eng. 167 (2020) 114806.
[9] J.M. Cardemil, A.R. Starke, A. Zurita, C. Mata-Torres, R. Escobar, Integration schemes for hybrid and polygeneration concentrated solar power plants, WIREs Energy Environ. 10 (2021) e412.
[10] M. Chitakure, W. Ruziwa, D. Musademba, Optimization of hybridization configurations for concentrating solar power systems and coal-fired power plants: A review, Renewable Energy Focus 35 (2020) 41–55.
[11] T. Yue, N. Lior, Thermal hybrid power systems using multiple heat sources of different temperature: Thermodynamic analysis for Brayton cycles, Energy 165 (2018) 639–665.
[12] H.G. Jin, H. Hong, Hybridization of concentrating solar power (CSP) with fossil fuel power plants, in: K. Lovegrove, W. Stein (Eds.), Concentrating Solar Power Technology, 12, Woodhead Publishing, 2012, pp. 395–420.
[13] R. Buck Bräuning T, Denk T, Pfänder M, Schwarzbözl P, Tellez F. Solar-Hybrid Gas Turbine-based Power Tower Systems (REFOS)* J. Sol. Energy Eng. 124 2001 2 9.
[14] P. Heller, M. Pfänder, T. Denk, F. Tellez, A. Valverde, J. Fernandez, et al., Test and evaluation of a solar powered gas turbine system, Sol. Energy 80 (2006) 1225–1230.
[15] U. Fisher, C. Sugarmen, A. Ring, J. Sinai, Gas Turbine "Solarization"-Modifications for Solar/Fuel Hybrid Operation, J. Sol. Energy Eng. 126 (2004) 872–878.
[16] Solgate. Solar Hybrid Gas Turbine Electric Power System. Technical Report EUR 21615 2005 European Commission Brussels Belgium.
[17] S. Pramanik, R.V. Ravikrishna, A review of concentrated solar power hybrid technologies, Appl. Therm. Eng. 127 (2017) 602–637.
[18] P. Schwarzbözl, R. Buck, C. Sugarmen, A. Ring, M.J. Marcos Crespo, P. Altwegg, et al., Solar gas turbine systems: Design, cost and perspectives, Sol. Energy 80 (2006) 1231–1240.
[19] R. Buck, S. Friedmann, Solar-Assisted Small Solar Tower Trigeneration Systems, J. Sol. Energy Eng. 129 (2007) 349–354.
[20] P. Garcia, A. Ferriere, G. Flamant, P. Costerg, R. Soler, B. Gagnepain, Solar Field Efficiency and Electricity Generation Estimations for a Hybrid Solar Gas Turbine Project in France, J. Sol. Energy Eng. 130 (2008).
[21] R. Korzynietz, J.A. Brioso, A. del Río, M. Quero, M. Gallas, R. Uhlig, et al., Solugas – Comprehensive analysis of the solar hybrid Brayton plant, Sol. Energy 135 (2016) 578–589.
[22] R. Korzynietz, M. Quero, R. Uhlig, Solugas – future solar hybrid technology, SolarPaces, Marrakech, Morocco, 2012.
[23] I. Hischier, P. Poživil, A. Steinfeld, Optical and Thermal Analysis of a Pressurized-Air Receiver Cluster for a 50 MWe Solar Power Tower, J. Sol. Energy Eng. 137 (2015).
[24] M.J. Santos, R.P. Merchán, A. Medina, H.A. Calvo, Seasonal thermodynamic prediction of the performance of a hybrid solar gas-turbine power plant, Energ. Conver. Manage. 115 (2016) 89–102.
[25] D. Olivenza-León, A. Medina, H.A. Calvo, Thermodynamic modeling of a hybrid solar gas-turbine power plant, Energ. Conver. Manage. 93 (2015) 435–447.
[26] R.P. Merchán, M.J. Santos, I. Reyes-Ramírez, A. Medina, H.A. Calvo, Modeling hybrid solar gas-turbine power plants: Thermodynamic projection of annual performance and emissions, Energ. Conver. Manage. 134 (2017) 314–326.
[27] R.P. Merchán, M.J. Santos, J. García-Ferrero, A. Medina, A.C. Hernández, Thermo-economic and sensitivity analysis of a central tower hybrid Brayton solar power plant, Appl. Therm. Eng. 186 (2021) 116454.
[28] J. Yang, G. Xiao, M. Ghavami, J. Al-Zaili, T. Yang, A. Sayma, et al., Thermodynamic modelling and real-time control strategies of solar micro gas turbine system with thermochemical energy storage, J. Clean. Prod. 304 (2021) 127010.
[29] G. Xiao, J. Chen, M. Ni, K. Cen, A solar micro gas turbine system combined with steam injection and ORC bottoming cycle, Energ. Conver. Manage. 243 (2021) 114032.
[30] M. Amani, A. Ghenaiet, Novel hybridization of solar central receiver system with combined cycle power plant, Energy 201 (2020) 117627.
[31] A. Ahmadi, M.A. Ehyaei, D.H. Jamali, M. Despotovic, F. Esmaeilion, A. Abdalisousan, et al., Energy, exergy, and economic analyses of integration of heliostat solar receiver to gas and air bottom cycles, J. Clean. Prod. 280 (2021) 124322.
[32] S.M. Alirahmi, A. Khoshnevisan, P. Shirazi, P. Ahmadi, D. Kari, Soft computing based optimization of a novel solar heliostat integrated energy system using artificial neural networks, Sustainable Energy Technol. Assess. 50 (2022) 101850.
[33] J. García-Ferrero, R.P. Merchán, M.J. Santos, A. Medina, H.A. Calvo, Brayton technology for Concentrated Solar Power plants: Comparative analysis of central tower plants and parabolic dish farms, Energ. Conver. Manage. 271 (2022) 116312.
[34] R. Ghasemiasl, H. Dehghanizadeh, M.A. Javadi, M. Abdolmaleki, 4E Transient Analysis of a Solar-Hybrid Gas-Turbine Cycle Equipped with Heliostat and MED, Sustainability. 15 (2023) 8792.
[35] F. Rovense, A. Sebastián, R. Abbas, M. Romero, J. González-Aguilar, Performance map analysis of a solar-driven and fully unfired closed-cycle micro gas turbine, Energy 263 (2023) 125778.
[36] K. Hemmatpour R. Ghasemiasl Malekzadeh dirin M, Javadi MA. Time-Transient Optimization of Electricity and Fresh Water Cogeneration Cycle Using Gas Fuel and Solar Energy Mathematics. 11 2023 571.
[37] R. Ghasemiasl, M. Khalili Abhari, M.A. Javadi, H. Ghomashi, 4E investigating of a combined power plant and converting it to a multigeneration system to reduce environmental pollutant production and sustainable development, Energ. Conver. Manage. 245 (2021) 114468.
[38] R. De Robbio, Micro Gas Turbine Role in Distributed Generation with Renewable Energy Sources, Energies 16 (2023) 704.
[39] J. Li, Y. Li, Micro gas turbine: Developments, applications, and key technologies on components, Propul. Power Res. 12 (2023) 1–43.
[40] A. Gouareh, B. Settou, N. Settou, A new geographical information system approach based on best worst method and analytic hierarchy process for site suitability and technical potential evaluation for large-scale CSP on-grid plant: An application for Algeria territory, Energ. Conver. Manage. 235 (2021) 113963.
[41] https://climate.onebuilding.org/.
[42] A.J. Hoshizaki, Operating Experience of the First Solar® Taurus 70S Mechanical Drive Installation. ASME 1997 International Gas Turbine and Aeroengine Congress and Exhibition, 1997.
[43] Y.A. Cengel, M.A. Boles, M. Kanoğlu, Thermodynamics: an engineering approach, 8th ed:, McGraw-hill New York, 2015.
[44] S. Campanari, L. Mastropasqua, M. Gazzani, P. Chiesa, M.C. Romano, Predicting the ultimate potential of natural gas SOFC power cycles with CO2 capture – Part A: Methodology and reference cases, J. Power Sources 324 (2016) 598–614.
[45] R. Pitz-Paal, ECOSTAR Roadmap Document 2005, Concrete (2003).
[46] J. Spelling, Hybrid solar gas-turbine power plants: a thermoeconomic analysis, KTH Royal Institute of Technology (2013).
[47] A. Belaid, A. Filali, S. Hassani, T. Arrif, M. Guermoui, A. Gama, et al., Heliostat field optimization and comparisons between biomimetic spiral and radial-staggered layouts for different heliostat shapes, Sol. Energy 238 (2022) 162–177.
[48] T. Arrif S. Hassani M. Guermoui A. Sánchez-González A. Taylor R, Belaid A. GA-GOA hybrid algorithm and comparative study of different metaheuristic population-based algorithms for solar tower heliostat field design Renew. Energy 192 2022 745 758.
[49] K. Deb, H. Jain, An Evolutionary Many-Objective Optimization Algorithm Using Reference-Point-Based Nondominated Sorting Approach, Part I: Solving Problems With Box Constraints, IEEE Trans. Evol. Comput. 18 (2014) 577–601.
[50] H. Jain, K. Deb, An Evolutionary Many-Objective Optimization Algorithm Using Reference-Point Based Nondominated Sorting Approach, Part II: Handling Constraints and Extending to an Adaptive Approach, IEEE Trans. Evol. Comput. 18 (2014) 602–622.
[51] S.Z. Mirjalili, S. Mirjalili, S. Saremi, H. Faris, I. Aljarah, Grasshopper optimization algorithm for multi-objective optimization problems, Appl. Intell. 48 (2018) 805–820.
[52] M.B. Ayhan, A fuzzy AHP approach for supplier selection problem: A case study in a Gear motor company, International Journal of Managing Value and Supply Chains. Vol. 4, No. 3 (2013).
[53] P. Kurup S. Akar S. Glynn C. Augustine P. Davenport Cost Update: Commercial and Advanced Heliostat Collectors. National Renewable Energy Lab 2022 (NREL), Golden, CO (United States).
[54] G. Zhu, C. Augustine, R. Mitchell, M. Muller, P. Kurup, A. Zolan, et al., HelioCon: A roadmap for advanced heliostat technologies for concentrating solar power, Sol. Energy 264 (2023) 111917.
[55] Irena Renewable power generation costs in 2022 2023 International Renewable Energy Agency Abu Dhabi.
[56] World Bank State and Trends of Carbon Pricing 2023 2023 World Bank Washington, DC 10.1596/978-1-4648-2006-9.
[57] Ember. Electricity generation by source. https://ember-climate.org/countries-and-regions/regions/middle-east/; 2022.
[58] M. Peyvandi, A. Hajinezhad, S.F. Moosavian, Investigating the intensity of GHG emissions from electricity production in Iran using renewable sources, Results Eng. 17 (2023) 100819.